Supporting Information

Reducing Nonradiative Losses in Perovskite Solar Cells via Ester-Based Lewis Base Passivation

Tunahan Akgul, [a] Murat Ebic,[b] Seckin Akin,[b,c] and Resul Ozdemir*[d]

[a] Department of Nanoscience and Nanotechnology, Graduate School of Natural and Applied Sciences, Eskisehir Osmangazi University, Eskisehir 26040, Türkiye

[b] Laboratory of Advanced Materials & Photovoltaics (LAMPs), Necmettin Erbakan University, Konya 42090, Türkiye

[c] Department of Metallurgy and Materials Engineering, Necmettin Erbakan University, Konya 42090, Türkiye

[d] Department of Electronics and Automation, Eskisehir Vocational School, Eskisehir Osmangazi University, Eskisehir 26110, Türkiye

*Address correspondence to: resul.ozdemir@ogu.edu.tr

1. Materials and Methods

All reactions involving air- or moisture-sensitive reagents were performed under an inert nitrogen atmosphere using standard Schlenk line techniques. Commercially available reagents and solvents were used as received unless further purification is specified. Melting points were measured using an Electrothermal IA9000 digital apparatus. Nuclear magnetic resonance (NMR) spectra were recorded on a JEOL ECZ500R spectrometer (^{1}H, 500 MHz; ^{13}C, 125 MHz). Elemental compositions were confirmed by microanalysis using a Leco Truspec instrument. Matrix assisted laser desorption/ionization time of flight mass spectrometry (MALDI TOF MS) data were obtained with a Bruker Microflex LT instrument. Thermal properties were evaluated by thermogravimetric analysis (TGA) and differential scanning calorimetry (DSC) using a PerkinElmer Diamond TG/DTA Thermal Analyzer and a PerkinElmer DSC8000, respectively, at a constant heating rate of 10 °C min^{-1} under a nitrogen atmosphere. UV–visible absorption spectra were acquired using a PerkinElmer Lambda 750 spectrophotometer, and infrared (IR) spectra were recorded with a PerkinElmer Spectrum Two

spectrometer in attenuated total reflectance (ATR) mode. Steady-state photoluminescence spectra were measured using a PerkinElmer LS-6500 fluorescence spectrometer.

2. Synthesis and Characterization

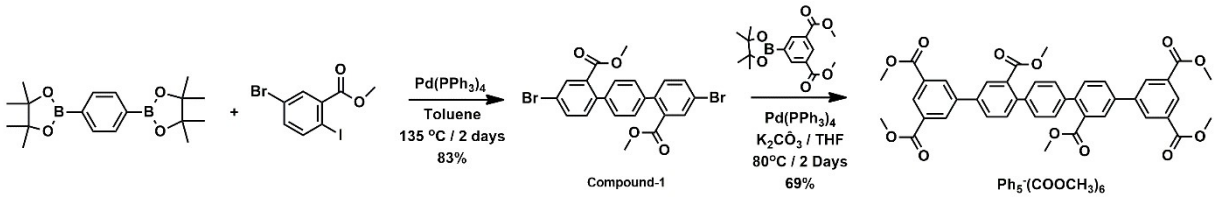

Scheme S1. Synthetic pathway of **Ph_5-$(COOCH_3)_6$.**

2a. Synthesis of dimethyl 4,4''-dibromo-[1,1':4',1''-terphenyl]-2,2''-dicarboxylate (Compound-1): A mixture of 1,4-benzenediboronic acid bis(pinacol) ester (2.518 g, 7.63 mmol), methyl 2-iodo-5-bromobenzoate (5.967 g, 16.71 mmol), and Aliquat 336 (0.801 g, 1.98 mmol) was suspended in 50 mL of degassed toluene under N_2. Then, tetrakis(triphenylphosphine)palladium (0.529 g, 0.458 mmol) and 1 M Na_2CO_3 solution (3.92 g in 32 mL of water), which was already degassed for 2 h, were added. Then, the reax. mixture was heated to 135 °C and stirred for 2 days. After completing the reaction, the mixture was cooled down to room temperature and quenched with water. Then, extracted with hexane, dried over Na_2SO_4, filtered, and evaporated to dryness to give the crude product. The crude was then purified by column chromatography on silica gel using chloroform as the eluent to give the pure product as a white solid (3.19 g, 83.0% yield). ^{1}H NMR (500 MHz, $CDCl_3$), δ (ppm): 3.67 (s, 3H), 7.28 (d, 3H, J = 5.0 Hz), 7.65 (dd, 1H, J = 10.0 Hz), 7.97 (d, 1H, J = 0 Hz).

2b. Synthesis of Hexakis(methoxycarbonyl)penta-1,1′:4′,1″:4″,1‴:4‴,1⁗-quinquephenyl (Ph_5-$(COOCH_3)_6$): The reagents dimethyl 4,4''-dibromo-[1,1':4',1''-terphenyl]-2,2''-dicarboxylate (Compound-1) (200 mg, 0.397 mmol), dimethyl 5-(4,4,5,5-tetramethyl-1,3,2-dioxaborolan-2-yl)isophthalate (280 mg, 0.875 mmol), and $Pd(PPh_3)_4$ (69 mg, 0.059 mmol) were dissolved in anhydrous THF (20 mL). Then, 1M K_2CO_3 degassed solution (560 mg in 4

mL of H_2O) was added. The reaction mixture was heated up to 80 °C and stirred for 2 days under N_2. After completing the reaction, the mixture was cooled down to room temperature and quenched with water. The reaction mixture was extracted with CH_2Cl_2, and the organic phase was washed with water, dried over Na_2SO_4, filtered, and evaporated to dryness to give the crude product. The crude product was then purified by column chromatography on silica gel using Ethyl Acetate: Hexane (1:1) as the eluent to afford the pure product as a pale pink solid (200 mg, 69% yield). Melting point: 247-248 °C. ^{1}H NMR (500 MHz, $CDCl_3$), δ (ppm): 8.69 (s, 1H), 8.53 (d, 2H J = 0 Hz), 8.13 (d, 1H, J = 5.0 Hz), 7.84 (dd, 1H, J = 10.0 Hz), 7.57 (d, 1H, J = 5.0 Hz), 7.42 (s, 2H), 3.99 (s, 6H), 3.74 (s, 3H). ^{13}C NMR (125 MHz, $CDCl_3$), δ (ppm): 60.5, 128.3, 128.7, 129.9, 131.5, 131.6, 132.3, 138.2, 139.9, 140.5, 141.9, 166.2. MALDI-TOF MS (positive mode) m/z $[M+Na]^+$: calcd for $C_{42}H_{34}O_{12}Na$: 753.20; found 753.06. Elemental analysis (%) calcd for $C_{42}H_{34}O_{12}$: C, 69.4; H, 4.69; O, 26.27; found: C, 68.91; H, 4.77.

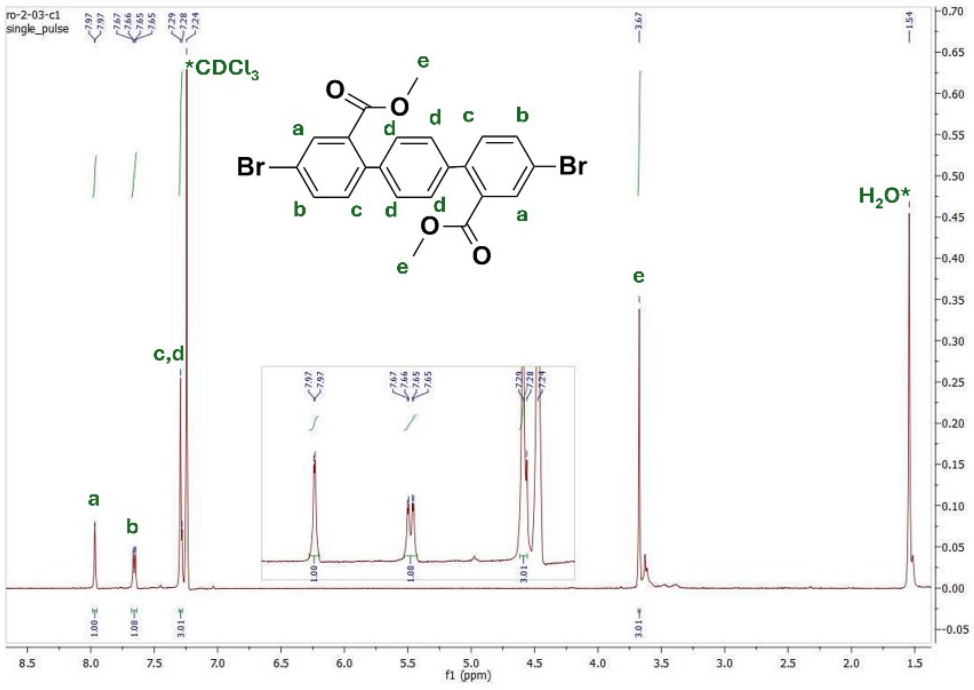

Figure S1. ^{1}H NMR spectra of Compound-1 in $CDCl_3$ measured at room temperature.

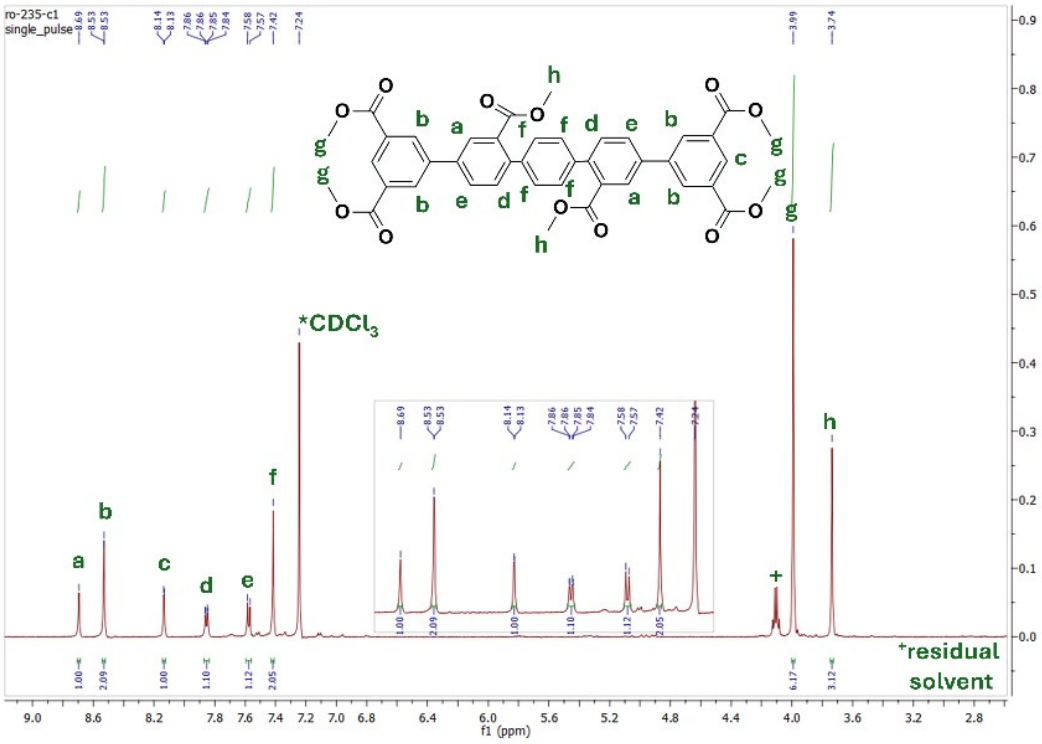

Figure S2. ^{1}H NMR spectra of Ph_5-$(COOCH_3)_6$ in $CDCl_3$ measured at room temperature.

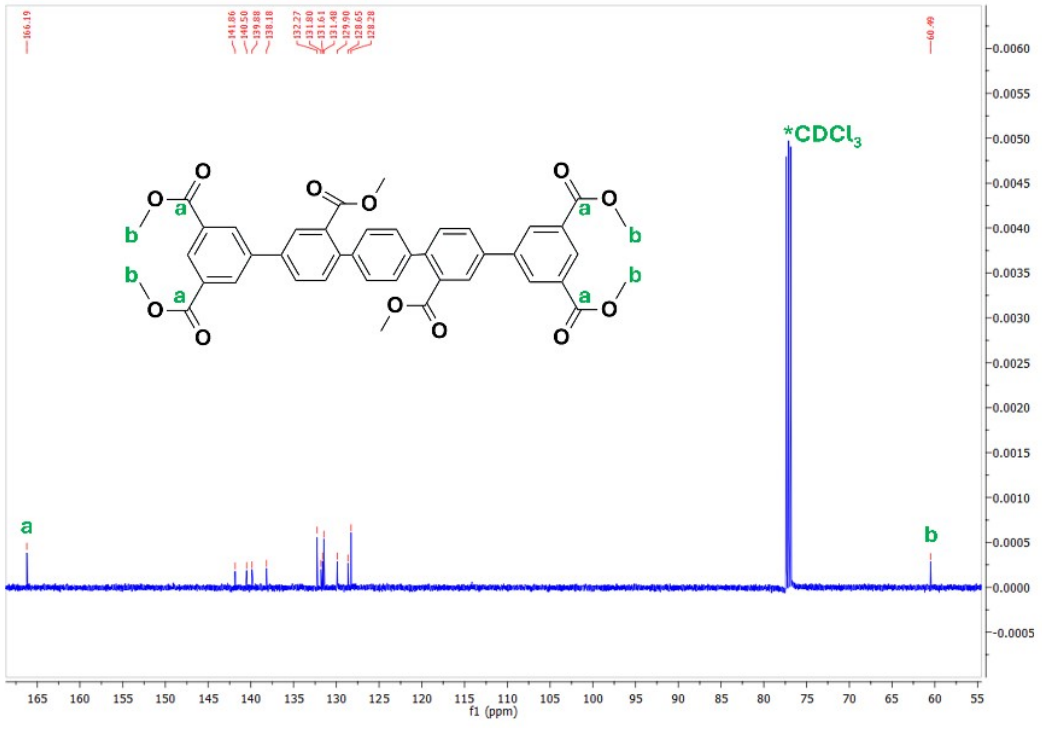

Figure S3. ^{13}C NMR spectra of Ph_5-$(COOCH_3)_6$ in $CDCl_3$ measured at room temperature.

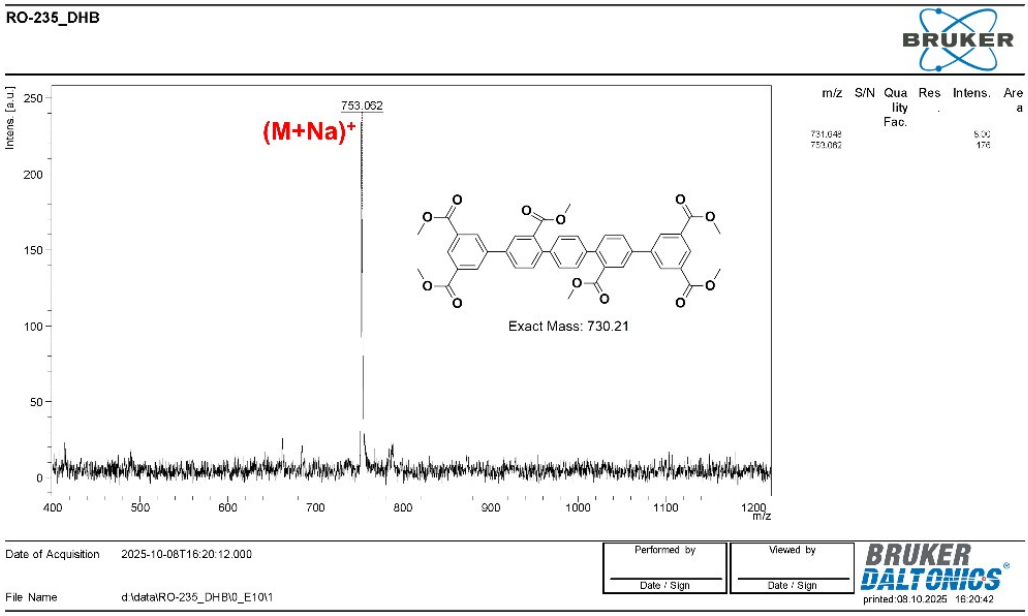

71

72 **Figure S4.** Positive ion and linear mode MALDI TOF-MS spectrum of Ph_5-$(COOCH_3)_6$.

73

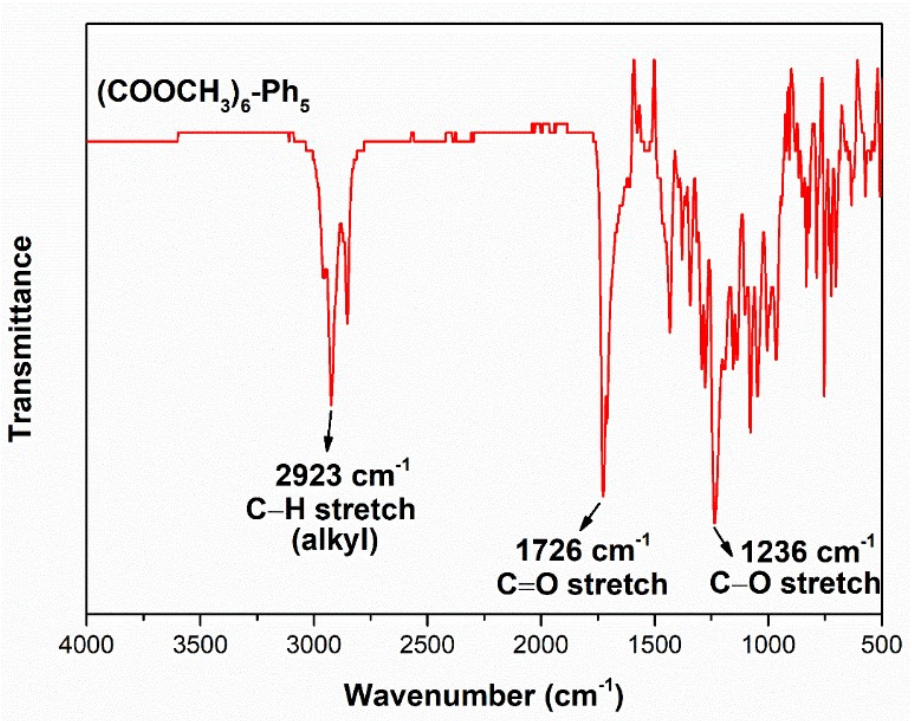

74

75 **Figure S5.** ATR FTIR spectra of Ph_5-$(COOCH_3)_6$ showing key stretching vibrational peaks.

76

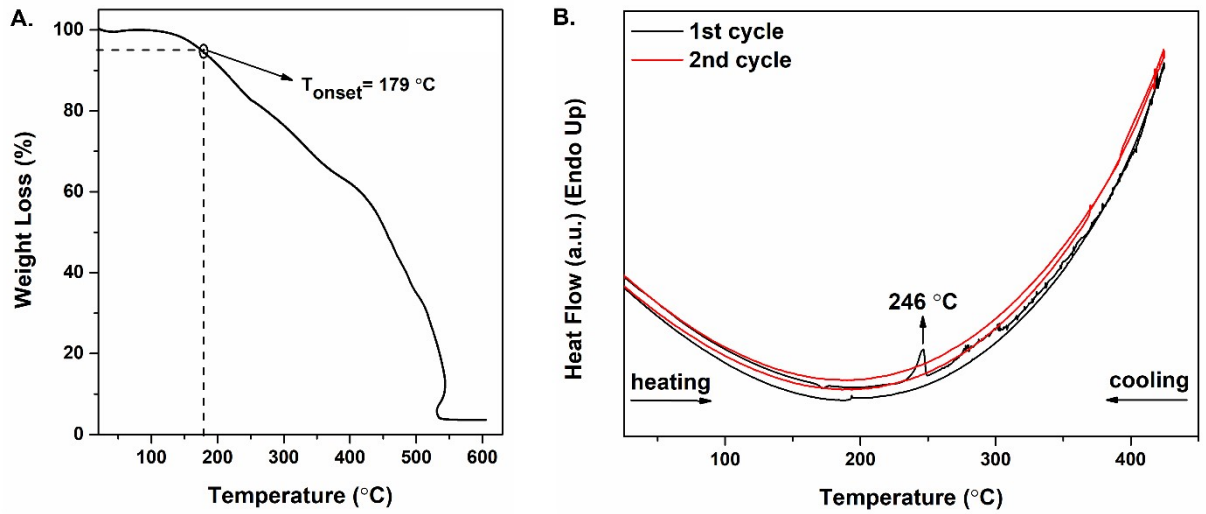

Figure S6. A) Thermogravimetric analysis (TGA) and B) differential scanning calorimetry (DSC) measurement curves in the first and second heating-cooling cycles for Ph_5-$(COOCH_3)_6$ at a temperature ramp of 10 °C min^{-1} under N_2.

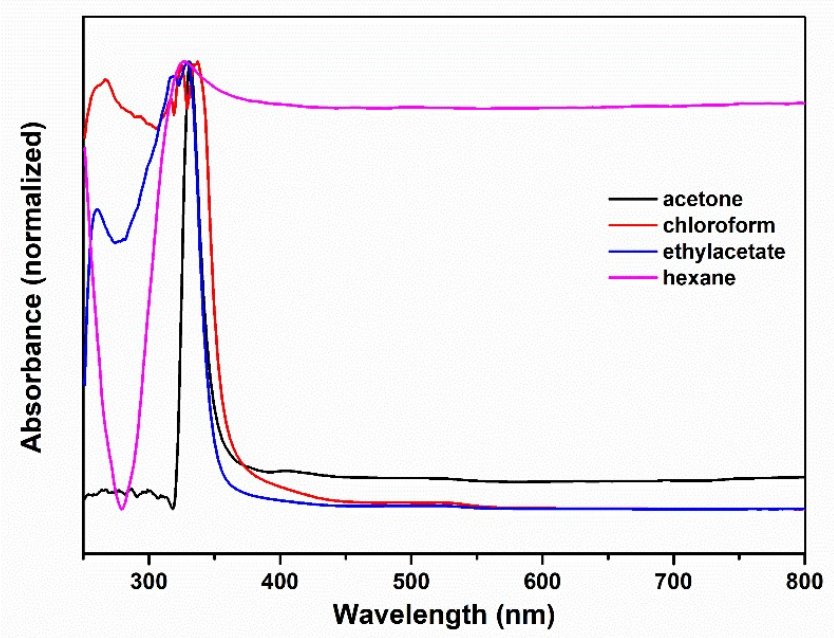

Figure S7. UV–vis absorption spectra of Ph_5-$(COOCH_3)_6$ recorded in four different solvents, hexane, chloroform, ethyl acetate, and acetone.

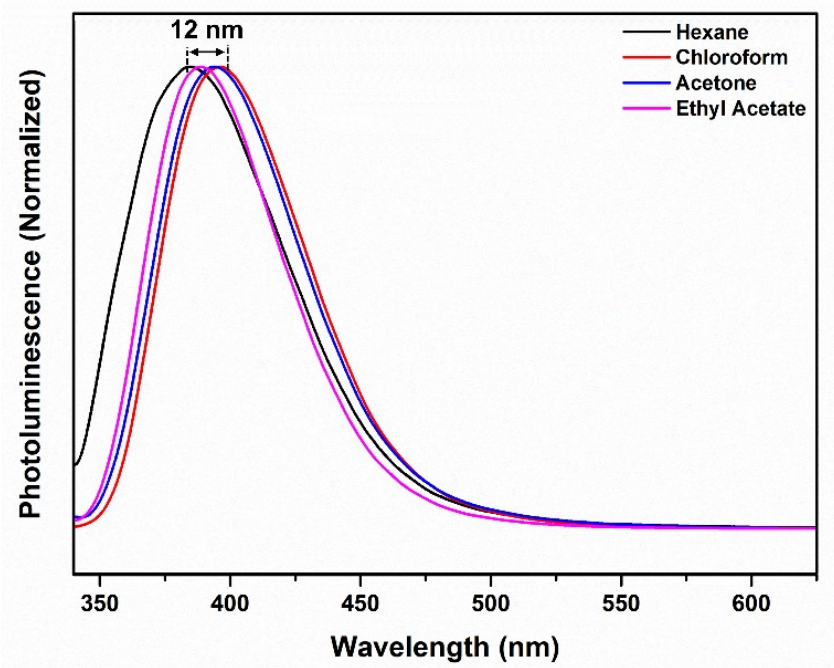

Figure S8. Photoluminescence (PL) spectra of Ph_5-$(COOCH_3)_6$ recorded in four different solvents, hexane, chloroform, ethyl acetate, and acetone.

3. Film and Device Fabrication Section

Substrate treatment: Commercial fluorine-doped tin oxide (FTO, sheet resistance ~7 Ω/sq, Asahi Glass) coated glass substrates were first patterned by chemical etching using zinc powder and 4 M hydrochloric acid. After patterning, the substrates were thoroughly cleaned in sequence with a detergent solution (Hellmanex), deionized water, acetone, ethanol, and 2-propanol under ultrasonic treatment. The cleaned substrates were subsequently dried by dry air flow.

Electron transport layers: A compact TiO_2 (c-TiO_2) hole-blocking layer was deposited using a precursor solution obtained by diluting titanium diisopropoxide bis(acetylacetonate) with acetylacetone in ethanol at a volume ratio of 1:9. Prior to deposition, the FTO substrates were treated with UV–ozone for 20 min (Jelight UV-Cleaner 24). The c-TiO_2 layer (~20 nm) was formed by oxygen-assisted spray pyrolysis at 450 °C, followed by annealing at the same temperature for 30 min. After an additional UV–ozone treatment, a mesoporous TiO_2 (mp-TiO_2) layer was deposited by spin-coating a TiO_2 paste diluted in absolute ethanol (1:6, w/w) at 5000 rpm for 10 s with an acceleration of 2000 rpm/s. The resulting films were thermally treated at 450 °C in dry air and subsequently transferred into a glovebox with relative humidity below 2% for perovskite deposition.

Perovskite absorber layer: The $FAPbI_3$ perovskite precursor solution was synthesized by dissolving formamidinium iodide (FAI) and lead iodide (PbI_2) at a stoichiometric 1:1 molar ratio in a mixed solvent system of anhydrous N,N-dimethylformamide (DMF) and dimethyl sulfoxide (DMSO). Methylammonium chloride (MACl) was introduced as a crystallization-modulating additive at a predetermined molar percentage relative to PbI_2. The total precursor concentration was adjusted to 1.4 M, and the solution was stirred at 60 °C for several hours until a clear and homogeneous solution was obtained, followed by filtration through a 0.45 μm PTFE syringe filter before use. The perovskite films were deposited on glass/FTO/c-TiO_2/mp-TiO_2 substrates using a two-step spin-coating protocol consisting of 2000 rpm for 10 s followed by 4000 rpm for 30 s. During the second step, 200 μL of chlorobenzene was dynamically dispensed approximately 10 s before the end of spinning to induce rapid crystallization. The coated films were annealed at 150 °C for 10 min and allowed to cool naturally to room temperature. For defect passivation, Ph_5-$(COOCH_3)_6$ was dissolved in 2-propanol and spin-coated directly onto the perovskite surface at concentrations of 1, 2, and 3 mg/mL. The deposition was carried out at 5000 rpm for 20 s. Following deposition, the passivated films were thermally treated at 100 °C for 10 min to promote solvent removal and enhance interfacial interaction between the passivation molecule and the perovskite layer.

Hole transport layer: The spiro-OMeTAD solution (70 mM) was prepared with lithium bis(trifluoromethanesulfonylimide) (Li-TFSI) and 4-tert-butylpyridine (tBP). The molar ratios of spiro-OMeTAD:Li-TFSI:tBP is 1.0:0.5:3.3. The HTL was deposited by spin coating at 5000 rpm for 20 s.

Top electrode deposition: A gold (~100 nm) electrode was thermally evaporated onto the HTL under high vacuum ($< 2 \times 10^{-6}$ Torr) using a VAKSİS MIDASm/PVD 40 system.

The device architecture in this study follows a conventional n-i-p configuration, with layer thicknesses controlled through established and reproducible fabrication protocols.

4. Thin-Film Characterization

XRD analysis: Structural analysis of the perovskite films was conducted using a PANalytical Empyrean diffractometer operating in Bragg–Brentano geometry with Cu $K\alpha_1$ radiation (λ = 1.5406 Å), an accelerating voltage of 40 kV, and a tube current of 30 mA. Diffraction patterns were recorded over a 2θ range of 10-40° with a step size of 0.01°.

XPS analysis: Surface chemical composition and electronic states were analyzed using XPS (TXPES Beamline at SESAME). Measurements were conducted under ultra-high vacuum (~10^{-7} mbar) with a flood gun. Binding energies were calibrated against the C 1s peak at 284.8 eV.

Optical spectroscopy: UV–Vis–NIR absorption spectra were collected at room temperature using a Shimadzu UV-1900i Plus spectrophotometer in the 400-850 nm wavelength range.

Morphological characterization: Surface morphologies were examined using a ZEISS GeminiSEM 500 SEM equipped with an InLens detector at an accelerating voltage of 1 kV.

AFM and KPFM: AFM measurements were carried out using a Park Systems XE7 instrument to obtain both 2D and 3D topographical images at scanning frequencies of 0.6–0.8 Hz. Surface roughness values were extracted using XEI software. KPFM was employed to probe photon-induced surface potential variations in both reference and IL-modified perovskite films.

PL and TRPL: Steady-state PL spectra were recorded with an Edinburgh Instruments FS5 spectrofluorometer using a 460 nm excitation source and monitoring emission between 700 and 850 nm. TRPL decay profiles were acquired using time-correlated single-photon counting, and the decay kinetics were fitted using a biexponential function. TRPL spectra were obtained with a pulsed 405 nm excitation from a pulsed solid state laser with pulse duration of about 1 ns. The results were calculated from a biexponentional fitting of TRPL spectra given by the following equation:

$$y = A_1 \cdot e^{-\left(\frac{x}{\tau_1}\right)} + A_2 \cdot e^{-\left(\frac{x}{\tau_2}\right)} \quad (1)$$

Where A_1 and A_2 are the relative amplitudes, and τ_1 and τ_2 represent the fast and slow decay components, respectively. The average carrier lifetime (τ_{av}) was calculated as the weighted mean of the two contributions: $\tau_{av} = (A_1 \cdot \tau_1) + (A_2 \cdot \tau_2)$.

5. Device Characterization

J–V measurements: Photovoltaic performance was evaluated using a solar simulator (ABET Sun 3000, AAA-rated) under AM 1.5G illumination at 100 mW/cm^2. Devices were masked to an active area of 0.09 cm^2 using an anti-reflective-coated black aperture. J–V curves were recorded with a Keithley 2400 source meter at a scan rate of 50 mV s^{-1}. Light intensity calibration and spectral mismatch correction were performed using a calibrated Si reference cell and a Schott KG-3 filter.

IPCE measurements: IPCE spectra were obtained under short-circuit conditions using a QEX10 system equipped with a xenon lamp, monochromator, and spectral response software.

EIS: Impedance measurements were conducted in the dark over a frequency range of 1 MHz to 1 Hz using an Ivium CompactStat potentiostat. The resulting spectra were fitted with equivalent circuit models to extract recombination-related parameters.

SCLC analysis: Trap density values were determined from dark I–V measurements of hole-only devices using the SCLC method.

M–S analysis: Carrier densities were extracted from capacitance–voltage measurements using M–S plots, where $1/C^2$ was plotted as a function of applied bias.

Stability evaluation: Operational stability was assessed using a Fluxim Litos Lite system under continuous white LED illumination (100 mW/cm^2) while tracking the maximum power point for up to 1000 h. All stability tests were conducted without encapsulation (at room temperature under nitrogen flow).

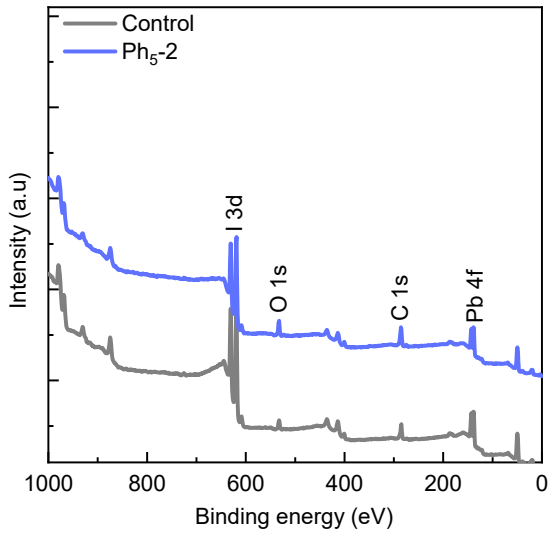

Figure S9. XPS survey spectra of control and Ph_5-2-passivated $FAPbI_3$ perovskite films.

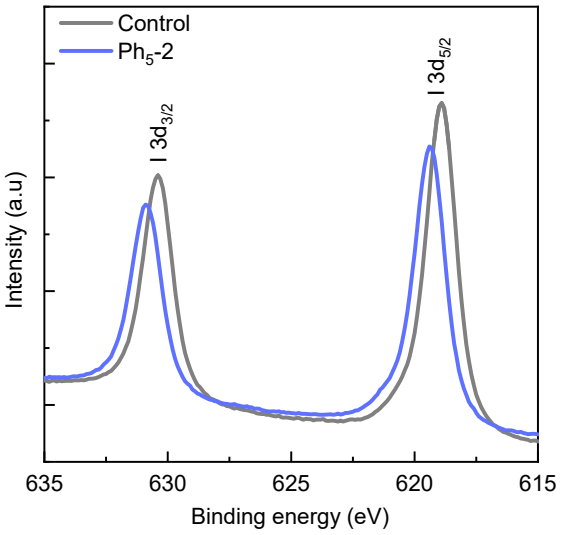

Figure S10. High-resolution I 3d XPS spectra of control and Ph_5-2-passivated $FAPbI_3$ perovskite film.

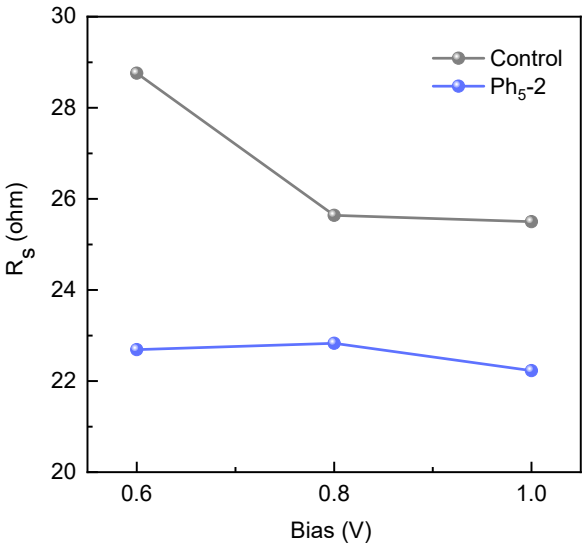

Figure S11. Bias-dependent series resistance (R_s) extracted from EIS measurements for control and Ph_5-2-passivated PSCs, plotted as a function of the applied bias voltage.

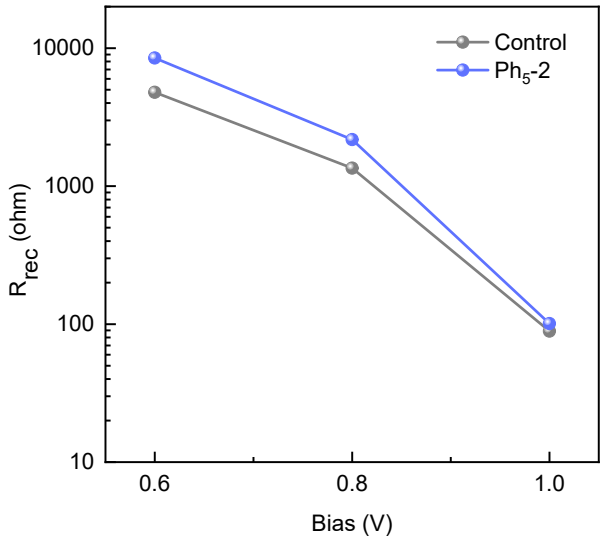

186

187 **Figure S12.** Bias-dependent recombination resistance (R_{rec}) extracted from EIS measurements
188 for control and Ph_5-2-passivated PSCs, plotted as a function of the applied bias voltage.

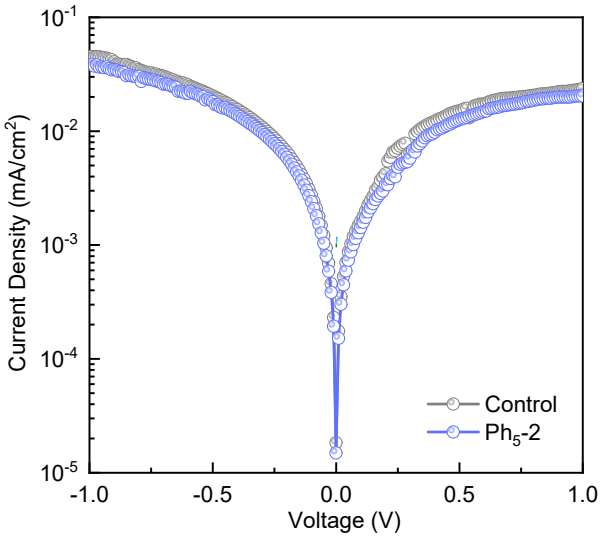

189

190 **Figure S13.** Dark J–V characteristics of control and Ph_5-2-passivated devices.

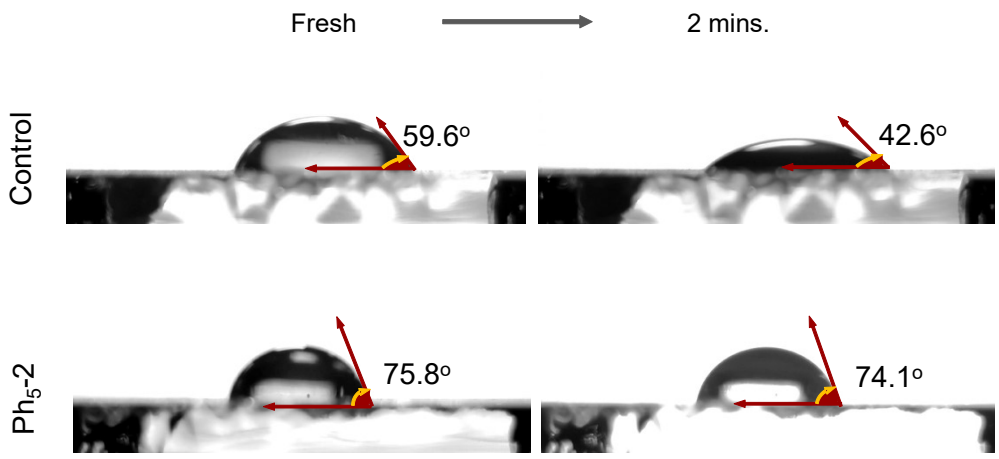

Figure 14. Time-dependent water contact-angle measurements of control and Ph_5-2-passivated perovskite films.

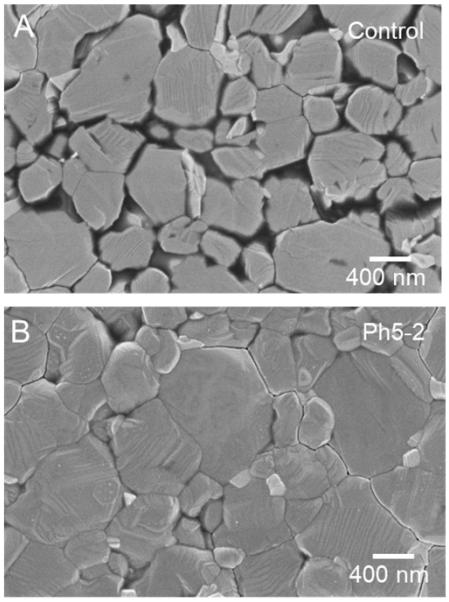

Figure S15. SEM images of aged perovskite films after 30 days of ambient storage without encapsulation. A) control and B) Ph_5-2-passivated perovskite films.

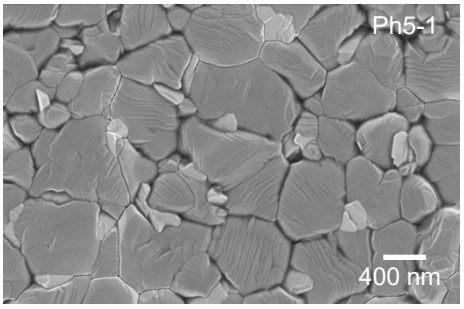

Figure S16. SEM image of aged Ph_5-1-passivated perovskite film after 30 days of ambient storage without encapsulation.

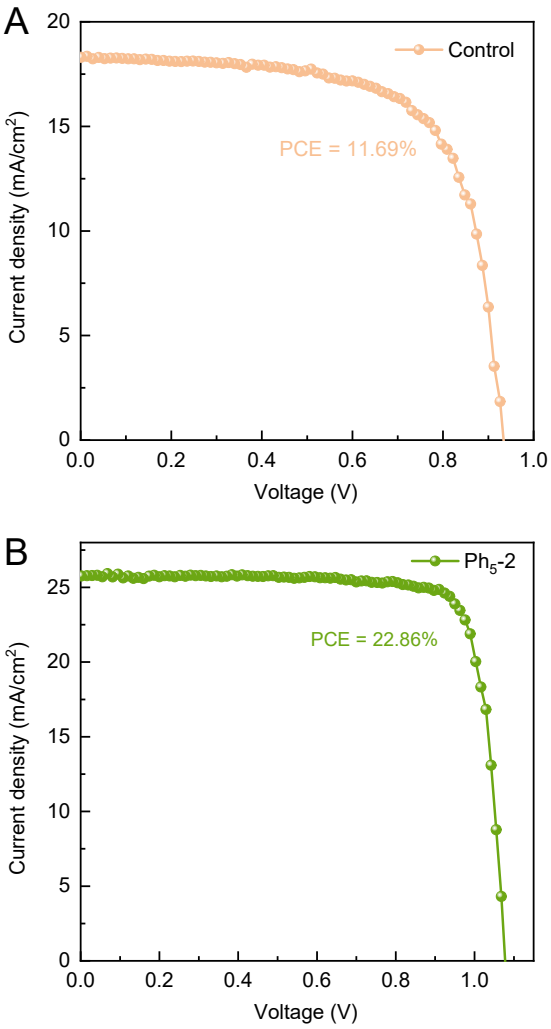

Figure S17. J–V characteristics of control and Ph_5-2-passivated devices measured after 30 days of ambient shelf-life storage at room temperature and 40% relative humidity without encapsulation.

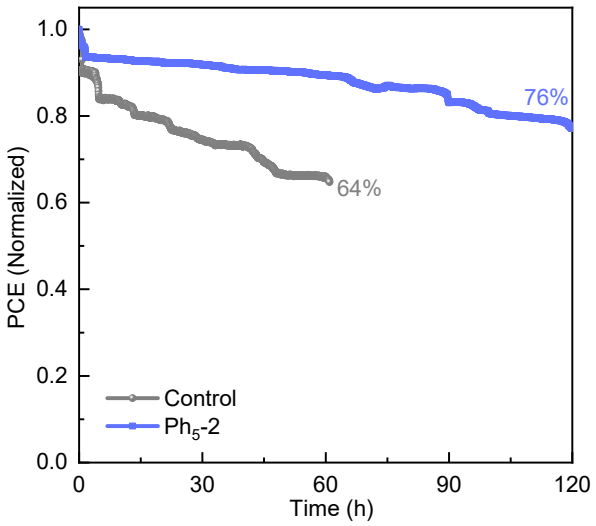

209

210 **Figure S18.** Thermal stability of control and Ph_5-2-passivated PSCs measured at 85 °C under
211 MPP conditions.

212

213 **Table S1.** Bi-exponential fitting parameters extracted from TRPL measurements of control and
214 Ph_5-2-passivated $FAPbI_3$ perovskite films without charge transport layers.

Sample	**A_1 (%)**	**τ_1 (ns)**	**A_2 (%)**	**τ_2 (ns)**	**τ_{av} (ns)**
Control	9.6	39.19	90.4	369.28	346.53
Ph_5-2	13.4	98.73	86.6	671.35	658.55

215

216